Proceedings of ISFOG 2025
5TH INTERNATIONAL SYMPOSIUM ON
FRONTIERS IN OFFSHORE GEOTECHNICS
Nantes, France | June 9-13 2025

ISBN 978-2-85782-758-0

Load capacity of deeply embedded tubular anchor in normally consolidated clay under inclined loading

S. Qin*, C.P. Aubeny
Texas A&M University, College Station, USA

J. Lee
Deep Anchor Solutions Inc., Houston, USA

M. Alessandrini
Global Maritime, Newcastle, UK

L. Huang, A. Martinez
University of California, Davis, USA

qinsong@tamu.edu

ABSTRACT: A deeply embedded tubular anchor is fully enveloped by soil, with the top of the anchor some 5-15 anchor diameters below the mudline. The deep embedment provides a high geotechnical efficiency such that a relatively compact anchor can provide high load capacity, thereby reducing fabrication, transport, and deployment costs, in addition to alleviating supply chain barriers and demands on the port facilities supporting wind and marine energy construction. This anchor can function in single-line and shared-anchor systems and is particularly promising for usage in taut mooring systems. In shared-anchor systems, the load inclination angle is variable, typically ranging from the mooring line attachment angle to nearly vertical. While deep embedment is possible in a variety of soil profiles, this study addresses load capacity in normally consolidated clay profiles. Optimal design of this anchor requires reliable estimates of ultimate load capacity over a range of load inclination angles. Toward this end, finite element (FE) studies were conducted to evaluate load capacity for loads ranging from purely vertical to purely horizontal. The vertical load capacity studies focus on establishing the conditions under which reverse end bearing resistance can be fully mobilized and determining the factors for forward and reverse end bearing resistance. The inclined and lateral loading studies quantified the effects of axial-lateral load interactions and rotational effects. Based on the finite element studies, an upper bound plastic limit analysis (PLA) formulation was developed to facilitate routine design calculations. FE and PLA solutions were validated through comparisons to geotechnical centrifuge test data.

Keywords: Deeply Embedded Tubular Anchor; Finite element analysis; PLA; Centrifuge test

INTRODUCTION

With about two-thirds of harvestable offshore wind being in water depths too deep for fixed foundations, floating offshore wind towers are expected to be a major player in the development of this resource. However, major cost reductions in the capital costs for floating offshore wind farm construction are needed to make these systems economically viable. This imperative motivated the development of a deeply embedded (5-15 diameters) tubular anchor concept (Figure 1), which produces a compact, high-capacity anchor. Its compactness also reduces fabrication, transport, and deployment costs, while alleviating supply chain challenges and easing pressure on port facilities supporting wind and marine energy construction (Lee and Aubeny, 2020; Lee et al., 2020; Qin et al., 2024). This anchor concept is likely to be most advantageous in taut and semi-taut mooring systems that impose an inclined load demand on the anchor. In shared-anchor systems, the resultant load inclination angle will be variable, ranging from physical mooring attachment angle to nearly vertical. Suction installation is possible in normally consolidated clays, while vibratory installation is envisioned for sand and interbedded sand-clay soil profiles. The installation feasibility of deeply embedded tubular anchor in clay has been evaluated in previous studies (Qin et al., 2025a, 2025b). This study focuses on load capacity in a soft clay seabed.

A deeply embedded anchor has some similarities to caisson anchors, in that both side resistance and end bearing contribute to vertical load capacity and horizontal load capacity is strongly influenced by anchor rotation. However, there are notable differences between the two anchors. For a

conventional caisson anchor, only reverse bearing resistance contributes to vertical capacity, while both forward and reverse bearing resistance contribute to vertical capacity of an embedded tube. Additionally, when suction (under-pressure inside of the caisson) is mobilized in a caisson anchor, bearing resistance mobilizes across the entire cross-section area of the caisson bottom. In contrast, bearing resistance in a deeply embedded tubular anchor only acts on the annulus area, raising concern about proving adequate vertical uplift capacity. Recent innovations in the tubular anchor design (patent pending) can effectively close off the base of the tube to ensure mobilization of bearing resistance across the entire cross-section bottom area. Regarding horizontal loading, the relatively short length of the embedded tube is likely to make it more susceptible to reductions in horizontal load capacity due to rotational effects. It is essential to comprehensively evaluate the vertical and horizontal capacities of deeply embedded tubular anchors in clay to ensure the stability of the mooring system. However, there is limited research to address this issue. This study investigates to evaluate the following for an embedded tube: (1) the forward and reverse end bearing resistance, (2) vertical load capacity for a closed versus open end, and (3) inclined load capacity for various pad-eye locations. The numerical investigation uses finite element (FE) analyses and an upper bound plastic limit analysis (PLA) formulation. Both FE and PLA results were validated through comparison with geotechnical centrifuge test data from Huang et al. (2025).

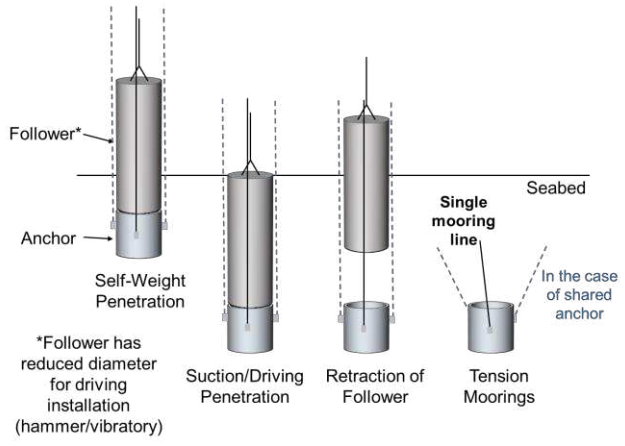

Figure 1. Deeply embedded tubular anchor and its installation procedure (Lee and Aubeny, 2020)

FINITE ELEMENT STUDY

Finite element (FE) analyses were conducted to evaluate the load capacity of the anchor in clay under loading conditions ranging from purely vertical to purely horizontal. The study analyzed the open-ended and closed-bottom cases, for pad-eyes located at the center and upper quarter points. The FE analysis was conducted using the commercial software package ABAQUS/Standard.

Three-Dimensional Model

The soil domain and anchor were discretized using continuum and hybrid elements (C3D8H) from the ABAQUS element library. Taking advantage of symmetry about the plane of loading, only half of the domain was modeled. The tubular anchor was represented as a rigid structure. Infinite elements (CIN3D8) were used to simulate far-field radial boundaries. The vertical displacement of the soil bottom is restrained. The mesh was refined both radially and vertically to improve computational efficiency, with element size increasing towards the boundaries. The minimum element size was set to 0.1 m. The anchor has an outer diameter, D, of 3 m, a wall thickness of 0.05 m, and an aspect ratio L/D = 2. Although early studies considered an aspect ratio of 1.5 (in the two-dimensional model analysis below), subsequent studies showed improved capacity with L/D = 2; thus, the current study adopts the larger aspect ratio. The soil domain diameter is approximately seven times the anchor diameter, with the anchor embedment depth set to 15 times the anchor diameter and the soil depth below the anchor extending to 5 times the anchor diameter. Movement at the bottom of the domain was fully restrained. Figure 2 shows the generated FE mesh, where D is the anchor outer diameter, t is the wall thickness, L is the anchor length, and z is the embedment depth of the bottom of the anchor.

Monotonic loading was applied using displacement control. Uniform displacement increments were applied at the pad-eye until a displacement of 10% of the anchor diameter was achieved in the loading direction. The anchor capacities are evaluated with varying loading directions, from 0° to 90° relative to horizontal, with 15° intervals. During loading, high stress concentrations typically develop around the top and bottom edges of the anchor, which can cause numerical convergence issues. To mitigate this, one ring of elements adjacent to the top and bottom tips of the anchor were modeled with reduced strength. The ring elements are in direct contact with the top and bottom anchor tips, with a breath equal to the wall thickness and a height of 0.1 m. The stress reduction factor in this region was set to 0.025. The undrained soil strength (S_u) of these elements is 0.025 times that of the surrounding soil at the same depth. The soil and anchor elements were assumed to be bonded together. To simulate the clay adhesion effect, soil elements

adjacent to the inner and outer walls of the anchor were assigned strength adhesion factors (α) of 0.65 and 0.75, respectively (Jeanjean, 2006; Jeanjean et al., 2006).

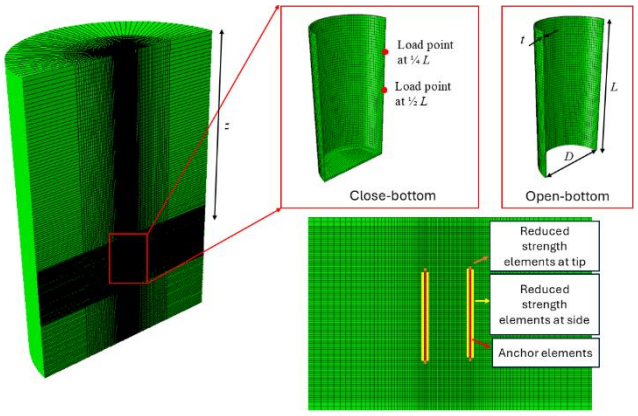

Figure 2. 3D FE mesh of the deeply embedded tubular anchor

Constitutive Behaviour and Strength Profile

The clay was modeled as an elastic-perfectly plastic material using the elastoplastic Mohr-Coulomb constitutive model. The angle of internal friction and the corresponding dilation angle were both set to 0°. The clay had a Poisson's ratio (v) of 0.49 and a Young's modulus (E) equal to 150 times the undrained shear strength (S_u). A soil profile with a linearly increasing undrained shear strength with depth was used, where the undrained shear strength at the soil surface was set to 0 kPa and the soil strength increased at a rate of 3.3 kPa/m.

Two-dimensional Axisymmetric Model

To evaluate vertical load capacity predictions from the 3D model, a series of analyses were also performed using a 2D axisymmetric model using the same anchor geometry and soil profile as the 3D model. The anchor and soil were discretized using axisymmetric hybrid elements (CAX4H). In this preliminary study, the anchor was modeled as a solid cylinder. The mesh around the anchor was refined to a minimum element size of 0.05 m.

Comparison of 2D Axisymmetric to 3D

Figure 3 shows Von Mises stress contours (front view) for both a 2D analysis of a solid cylinder and a 3D analysis of an open bucket with a solid bottom. The gray part represents the anchor. The stress distribution in the figure shows the soil beneath the anchor is subject to high stresses under vertical loading. The vertical capacity obtained from the 2D model (19,200 kN) was 4.7% higher than that from the 3D model (18,300 kN). Since the tubular anchor in the 3D analysis had an open top, while the axisymmetric model used a solid cylinder, the reduced vertical capacity from the 3D model may be attributed in part to the soil compressibility inside the bucket.

To evaluate the vertical end bearing factor, N_a, from the FE predictions, the following equation was used to separate the bearing and side friction components of resistance:

$$N_a = (Q_{total} - Q_{side})/(S_{uavg} * A_b) \qquad (1)$$

where Q_{total} is the ultimate vertical capacity, Q_{side} is the side frictional force, S_{uavg} is the average of the undrained shear strength at the tip and top of the anchor, and A_b is the bearing area. For an open tube A_b equals the annular area, while for the closed bottom it equals the total cross-sectional area. The side friction Q_{side} calculation assumes that full frictional resistance, αs_u, mobilizes along the entire exterior and interior surfaces (only exterior surface for anchor with closed bottom). N_a values back calculated from 2D FE analyses of anchors with aspect ratios L/D = 1.5 and 2 were 6.80 and 6.79, respectively. Hence, the aspect ratio appears to have a minor effect on the end bearing factor. The theoretical end bearing factor (Martin and Randolph, 2001) for a circular disc (L/D = 0) implies 6.2 for α = 0 to 6.5 for α = 1 for forward and reverse end bearing. Thus, the FE approximation appears to slightly overestimate the reference value, by about 5%.

N_a back calculated from the 3D model was 6.4, about 5% less than the 2D analysis for a solid cylinder. Recalling that the 3D analysis was for an open bucket with a closed bottom, this difference is attributed to the compressibility of the soil inside the bucket.

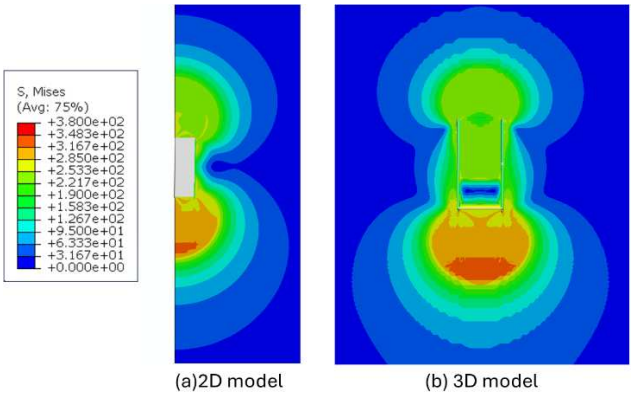

Figure 3. Von Mises stress contours: (a)2D axisymmetric model; (b) 3D model

PLASTIC LIMIT ANALYSIS

Aubeny et al. (2001, 2003) developed upper bound plastic limit analysis (PLA) solutions for caissons

subjected to horizontal and inclined loads. PLA solution was developed to estimate the ultimate load capacity of caissons and short piles. For the present study, this analysis was modified (Figure 4) to include vertical resistance from forward bearing and rotational resistance from a hemispherical slip surface at the top of the embedded tube. The PLA was also modified to consider both solid cylinders and hollow tubes. Based on the discussion in the previous section, forward and reverse end bearing factors of closed-bottom anchor under pure vertical loading was taken as N_a = 6.4. Open-ended tube analyses used an annular bearing factor N_a = 7.3.

The original analyses by Aubeny et al. (2001, 2003) incorporated free surface effects, including gapping and reduced soil resistance, into the lateral resistance calculation. The modified model for the deeply embedded tube retains these features; however, free surface effects have reduced or even no impact on deeply embedded tube behavior.

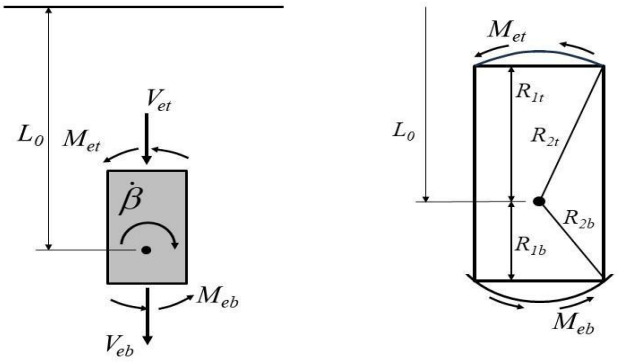

Figure 4 End resistance in the PLA model

The study compared the ultimate load predictions from the Plastic Limit Analysis (PLA) with those from 3D finite element (FE) analysis for varying load inclination angles from 0 to 90°. Anchors with both solid and open bottoms were analyzed (Figure 5). For loads attached at ½ *L* to an open-bottom anchor, the FE model predictions exceed the PLA values by about 17% for pure vertical and pure horizontal loading. Further, the PLA shows a trend at shallow load angles that differs from the FE predictions, with a reduced horizontal load capacity occurring for load inclinations less than about 10°. Comparing the open tube to a solid-bottom anchor, the PLA model predicts an increase in vertical load capacity of more than 50%, while the FE model predicts an increase of only 26%. This may be due in part to the fact that the load is applied at the wall, so loading is not purely vertical, but combined with vertical-moment loading. The FE model apparently predicts a greater vertical-moment interaction effect than the PLA.

For the case of loading point is at ¼ *L* from the top of the anchor, the FE model predicted horizontal capacity exceed the PLA value by about 17% higher than the PLA prediction. In this case both FE and PLA show trends of reduced horizontal capacity at shallow load angles. For the open-ended anchor, both PLA and FE show virtually no interaction effects (a flat yield locus) for load inclination angles exceeding 45°. For the solid-bottom case, the load attachment at the wall again seems to induce a vertical-moment interaction effect, with a modest reduction in vertical load capacity. It is noted that purely vertical eccentric loading of a tube anchor rarely occurs in practice. In single-line anchors in a taut or semi-taut, the load angle equals the physical load attachment angle, which is well below 90°. In shared-anchor systems, the resultant load inclination angle can approach 90°, but this load passes through the anchor centerline.

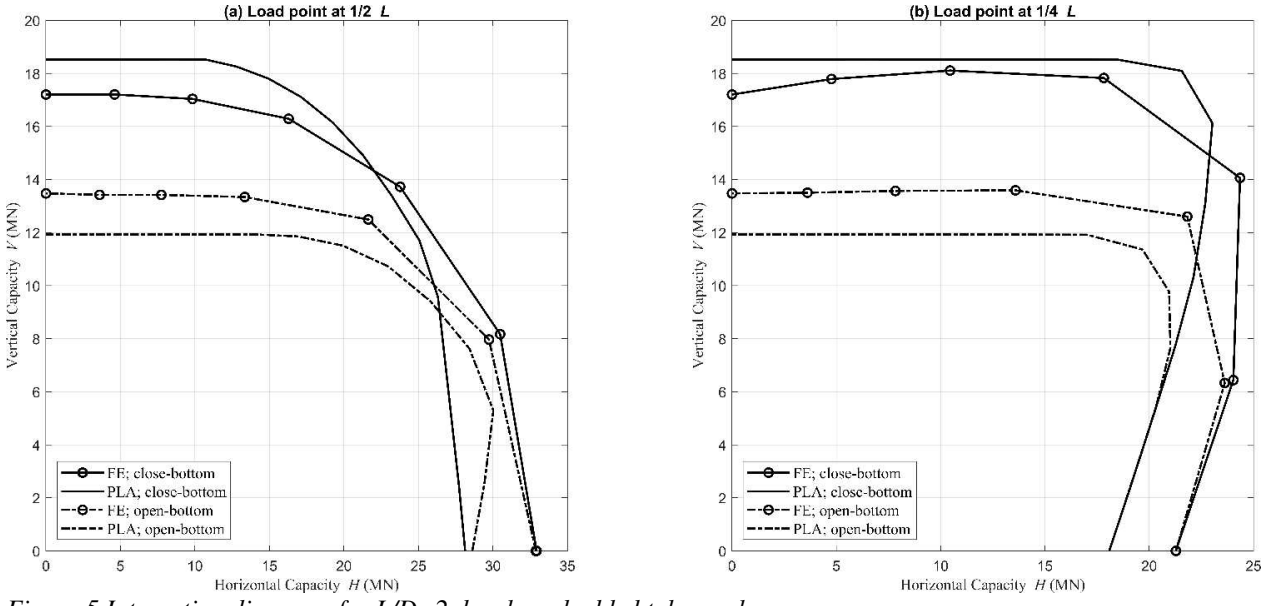

Figure 5 Interaction diagrams for L/D=2 deeply embedded tube anchor

COMPARISON TO EXPERIMENTAL DATA

Centrifuge tests conducted at the Center for Geotechnical Modelling (CGM) at the University of California, Davis (Huang et al., 2025) at an applied gravity of 70g for 30 to 90° load angles. The tests were carried out on a 2.8-m diameter by 4.2-m long (prototype scale) tubular anchor with the tip embedded 12.6 m ("shallow") and 21 m ("deep") below the mudline. The pad-eye was attached 1.26 m below the anchor top. T-bar undrained shear strength measurements showed a surface crust, with linearly varying strength in the underlying soil. Strength profiles in the sub-crustal soils (i.e. surrounding the anchor) could be described by lines with zero intercept and gradients of 2.8-5 kPa/m, with an average of 3.3 kPa/m. PLAs were therefore conducted for the anchor geometry and depths described above for the low (2.8 kPa/m), average (3.3 kPa/m), and high (5 kPa/m) estimate undrained strength profiles (Figure 6). The ultimate capacities of the anchor were estimated for a sweep of load inclination angles from 0-90°, as shown in Figure 6. For the shallow embedment case, measured capacities were between the average and high PLA predictions, indicating a possible effect of the overconsolidated crust. For deep embedment, measurements matched the average PLA predictions reasonably well.

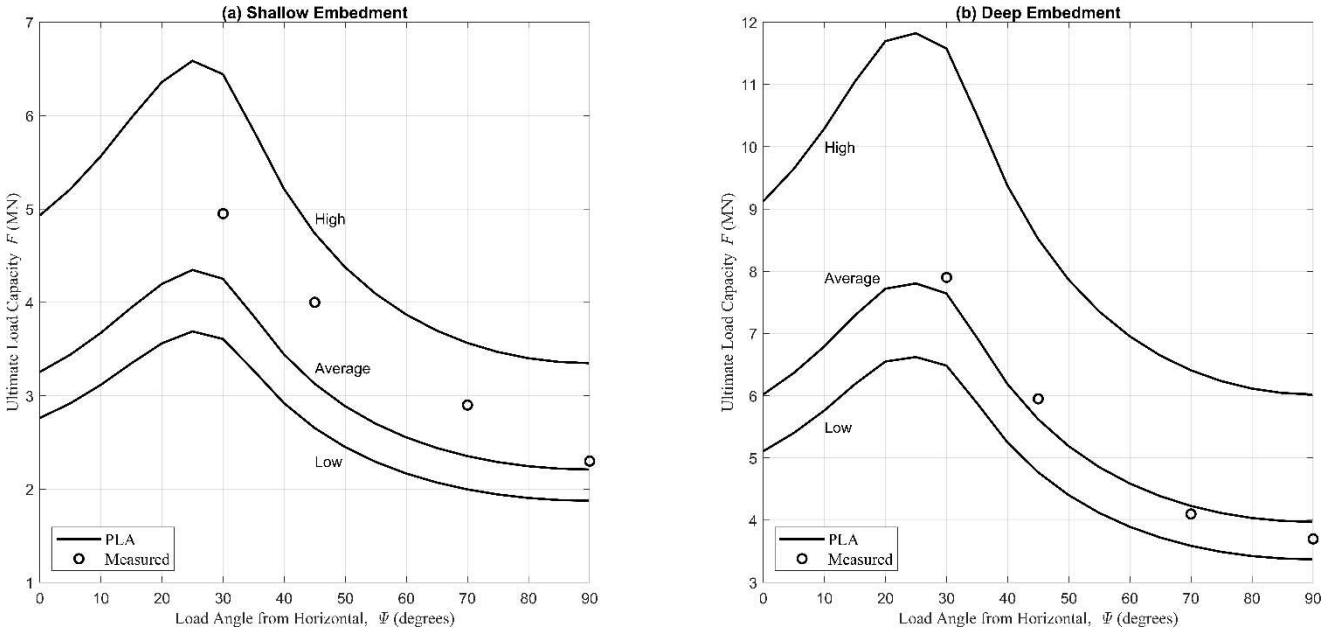

Figure 6 Comparison of PLA predictions to measured load anchor capacity

CONCLUSIONS

This study employed FE, PLA and centrifuge tests to evaluate various aspects of estimating ultimate load capacity for a deeply embedded tube anchor subjected to vertical and inclined loads. Open and closed-bottom tubes were considered in the numerical studies. Significant conclusions are as follows:

- An annular bearing factor for vertical load capacity N_a = 7.3 for forward and reverse end bearing of an open-ended tube anchor produce PLA predictions consistent with centrifuge test data.
- In agreement with the Randolph-Martin (2001) plastic limit solutions for a thin circular disk, N_a = 6.2-6.5, the FE analysis provides a reasonable basis for estimating the forward and reverse end bearing resistance of a tube anchor with a solid bottom.
- The FE predictions indicate that the vertical-moment interaction effect can reduce the vertical load capacity of a deeply embedded tubular anchor when the load is near vertical and attached to the wall. However, purely vertical eccentric loading seldom occurs in either single-line or shared-anchor systems.
- FE predictions of horizontal and inclined load capacity exceed PLA predictions by somewhat more than 15%. Since horizontal load capacity in PLA calculations is derived from a very sound basis, the Randolph and Houlsby (1984) plastic limit solutions for a translating cylinder, it is recommended that greater credence should be

given to the PLA solutions, unless future measurements suggest otherwise.

- The PLA solution provided estimates that agreed with centrifuge load tests performed at angles between 30° and 90°, further providing confidence in the solution's accuracy.

AUTHOR CONTRIBUTION STATEMENT

S. Qin: FE Analysis, Writing- Original draft, Editing. **C.P. Aubeny**.: Revise draft, PLA Analysis, Methodology. **J. Lee**: Writing-Reviewing; Supervision. **M. Alessandrini**: Supervision **L. Huang and A. Martinez**: Centrifuge tests.

ACKNOWLEDGEMENTS

The authors would also like to acknowledge the supports from the National Science Foundation, award numbers CMMI-1936901, CMMI-1936939, and TI-2214009, and the Department of Energy, award numbers DE-SC0024062 and DE-EE0011636.

REFERENCES

Aubeny, C. P., Han, S. W., & Murff, J. D. (2003). Inclined load capacity of suction caissons. *International Journal for Numerical and Analytical Methods in Geomechanics*, *27*(14), 1235-1254. https://doi.org/10.1002/nag.319

Aubeny, C. P., Murf, J. D., & Moon, S. K. (2001). Lateral undrained resistance of suction caisson anchors. *International Journal of Offshore and Polar Engineering*, *11*(03).

Huang L, Martinez A, Aubeny C, Arwade S, DeGroot D, and Beemer R (2025) Centrifuge Modelling of the Monotonic Capacity of Offshore Ring Anchors in Clay, GeoFrontiers 2025.

Jeanjean, P. (2006, May). Setup characteristics of suction anchors for soft Gulf of Mexico clays: Experience from field installation and retrieval. In *Offshore Technology Conference* (pp. OTC-18005). OTC.

Jeanjean, P., Znidarcic, D., Phillips, R., Ko, H. Y., Pfister, S., Cinicioglu, O., & Schroeder, K. (2006, May). Centrifuge testing on suction anchors: Double-wall, over-consolidated clay, and layered soil profile. In *Offshore Technology Conference* (pp. OTC-18007). OTC.

Lee, J., & Aubeny, C. P. (2020). Multiline Ring Anchor system for floating offshore wind turbines. In *Journal of Physics: Conference Series* (Vol. 1452, No. 1, p. 012036). https://doi.org/10.1088/1742-6596/1452/1/012036

Lee, J., Khan, M., Bello, L., & Aubeny, C. P. (2020). Cost analysis of multiline ring anchor systems for offshore wind farm. In *Proc., Deep Foundation Institute 45th Conference* (pp. 484-493).

Martin, C. M., & Randolph, M. F. (2001, January). Applications of the lower and upper bound theorems of plasticity to collapse of circular foundations. In *Proc., 10th Int. Conf. on Computer Methods and Advances in Geomechanics* (Vol. 2, pp. 1417-1428). Abingdon, England: Taylor & Francis.

Qin, S., Lee, J. & Aubeny, C.P. Fatigue performance of the Deeply Embedded Ring Anchor. Geo-Engineering 15, 23 (2024). https://doi.org/10.1186/s40703-024-00224-2

Qin, S., Lee, J., & Aubeny, C.P. (2025a). Evaluation of the Feasibility and Effectiveness of the Impact Hammer Installation of Deeply Embedded Ring Anchor. In *Geotechnical Frontiers 2025* (pp. 114-123).

Qin, S., Lee, J., & Aubeny, C.P. (2025b). Overcoming stiff clay anchoring challenges through vibratory installation with a Deeply Embedded Ring Anchor. In *Geo-Extreme 2025*. [forthcoming].

Randolph, M. F., & Houlsby, G. T. (1984). The limiting pressure on a circular pile loaded laterally in cohesive soil. *Geotechnique*, *34*(4), 613-623. https://doi.org/10.1680/geot.1984.34.4.613